

Mode Decomposition for Homogeneous Symmetric Operators*

Ido Cohen[†] Omri Azencot[‡] Pavel Lifshits[†]
 Guy Gilboa[†]

July 19, 2022

Abstract

Finding latent structures in data is drawing increasing attention in broad and diverse fields such as fluid dynamics, signal processing, and machine learning. In this work, we formulate *Dynamic Mode Decomposition* (DMD) for two types of dynamical system. The first, a system which is derived by a γ -homogeneous operator ($\gamma \neq 1$). The second, a system which can be represented as a symmetric operator.

Regarding to the first type, dynamical systems, derived by γ -homogeneous operators $\gamma \in [0, 1)$, reach the steady state in finite time. This inherently contradicts the DMD model, which can be seen as an exponential data fitting algorithm. Therefore, the induced DMD operator leads to artifacts in the decomposition. We show certain cases where the DMD does not even exist. For homogeneous systems ($\gamma \neq 1$), we suggest a time rescaling that solves this conflict and show that DMD can perfectly restore the dynamics even for nonlinear flows. For dynamics which derived by a symmetric operator, we expect the eigenvalues of the DMD to be real. This requirement is embeded in a variant of the DMD algorithm, termed as *Symmetric DMD* (S-DMD).

With these adaptations, we formulate a closed form solution of DMD for dynamics $u_t = P(u)$, $u(t=0) = u_0$, where P is a nonlinear γ -homogeneous operator, when the initial condition u_0 admits the nonlinear eigenvalue problem $P(u_0) = \lambda u_0$ (u_0 is a nonlinear eigenfunction, with respect to the operator P). We show experimentally that, for such systems, for any initial condition, S-DMD achieves lower mean square error for

*Ido would like to thank Prof. Andrea Bertozzi for the opportunity of studying in mathematics science department, UCLA in general and for helpful conversations, related to this work, in particular. **Funding:** This work was supported by the European Union's Horizon 2020 research and innovation programme under the Marie Skłodowska-Curie grant agreement No. 777826 (NoMADS). GG acknowledges support by the Israel Science Foundation (Grant No. 534/19) and by the Ollendorff Minerva Center.

[†]Electrical Engineering Department at the Technion – Israel Institute of Technology (idoc@campus.technion.ac.il, pavel@ee.technion.ac.il, guy.gilboa@ee.technion.ac.il).

[‡]Department of Mathematics, University of California Los Angeles (azencot@math.ucla.edu).

the spectrum estimation. Finally, we formulate a discrete decomposition, related to nonlinear eigenfunctions of γ -homogeneous operator.

Keywords— nonlinear decomposition, dynamic mode decomposition, homogeneous operators, monotonically decaying flows

1 Introduction

Finding latent structures in data is an essential task in diverse fields, from signal processing through [1] fluid dynamics analysis [2] to machine learning [3]. These structures commonly stand in the center of broad applications such as denoising, forecasting and classifying [4] to name a few. These structures get different forms in different disciplines. For example, in image processing, the structures can be the probabilistic of repetitive patches in different scales [5], in signal processing they can be a sum of eigenfunctions [6], in fluid dynamics the structures are represented as a sum of modes [7] and in machine learning they might be recurrence of words [8]. Despite of this diversity, different techniques from different disciplines might share similar principles.

In this work, we formulate a signal decomposition framework, related to the eigenfunctions of γ -homogeneous operators, using insights from fluid dynamics and based on dynamic mode decomposition [7]. Our analysis shows that DMD produces inaccurate estimations when applied to uniformly sampled observations of nonlinear homogeneous flows. Thus, we suggest an adaptive sampling rate that allows DMD to fully recover the underlying dynamics. Moreover, as our flows are governed by operators with real-valued spectrum, we propose a new method named *Symmetric DMD* (S-DMD) which guarantees that the output matrix is symmetric.

Recently, a new signal decomposition, related the eigenfunction of the γ -homogeneous operator, P ($\gamma \in (0, 1)$), was first introduced in [9]. This decomposition is based on the analysis of the solution to the PDE

$$\psi_t = P(\psi), \quad \psi(t = 0) = f.$$

It was found that the solution of this equation has finite support in time. Namely, the solution reaches its steady state in finite time. Moreover, the solution is variable separated when f is an eigenfunction of P , i.e. f admits the nonlinear eigenvalue problem $P(f) = \lambda \cdot f$ [10]. Following these attributes of the solution, the authors of [10] formulated a nonlinear spectral decomposition framework. This framework reveals the structures that stay unchanged under the flow. It generalized the previous study [11][12], focused on zero-homogeneous operators which are variational derivatives of absolutely one-homogeneous functionals.

The basis of this decomposition is the amplitude change rate of a signal under the flow, termed as the *decay profile*. Knowing the decay profile and the time of convergence to steady state, different modes of the signal can be distinguished. In addition, the decay profile might reveal the scale of the spatial structure. This concept was generalised in [13, 14]. In this work, the authors suggested to find a dictionary of decay profiles that compactly represents the dynamics. Relating different parts of the signal to the same decay profile reveals and connects between latent structures and scale within a signal.

In the fluid dynamics community, finding modes has drawn research attention for decades. A particularly successful approach in this context is based on the relation between Koopman theory [15, 16] and dynamical systems. In practice, an approximation of the linear yet infinite-dimensional Koopman operator can be computed using

the Dynamic Mode Decomposition method [7] which combines dimensionality reduction with a linear solve. Several works have shown that DMD is an effective tool for analyzing various aspects of nonlinear flows including their decay profiles [17, 18, 19].

However, the baseline DMD algorithm was shown to be sensitive to noisy data [20]. Specifically, DMD produces a systematic bias in its spectrum estimates which is not alleviated when more data is present [21]. The effect of small sensor noise on DMD and the Koopman expansion has also been explored and characterized [22]. Several attempts have been made to debias DMD with respect to noise including the use of the forward and backward dynamics [23], formulating the problem as a total least squares optimization [21], and using a variational approach [24]. The authors in [25, 26] used Kalman filters to cope with the noise, and Williams et al. [27] suggested to extend the basis of the sampled data snapshots, while [28] uses deep learning to learn the basis dictionary of the operator. More recent approaches harness the benefits of neural networks to propose effective Koopman-based designs [29]. In this work, we incorporate prior knowledge about the dynamics and their spectrum. In our approach, we utilize prior known information about the spectrum and force an algebraic form of the estimated operator, in some sense this approach is close to [17] where exponential model was fitted. We formulate the *Symmetric DMD* (S-DMD), which is DMD when the matrix has only real eigenvalues.

Main contributions and structure of the paper In this work, we study the connections between dynamic mode decomposition and nonlinear spectral analysis of γ -homogeneous flows. Our contributions can be summarized as follows.

First, we initialize a flow with a nonlinear eigenfunction, showing that DMD is not applicable in this setting. Nevertheless, a temporal re-parametrization of the data sampling leads to DMD results that are identical to previous spectral decompositions [9].

Second, we suggest a particular re-scaling of the time axis [30] such that a unique DMD solution is obtained. Our re-scaling yields an exponentially decaying solution, even though the operator P is nonlinear.

Third, for dynamics with a real-valued spectrum, we improve the baseline DMD which may produce complex values in the noisy setting by proposing the S-DMD variant which yields symmetric operators.

Finally, we show how the nonlinear spectral framework of [9] can be approximated with our tools orders of magnitude faster compared to previous work.

Our paper is organized as follows. We briefly describe some of the necessary components and background in Sec. 2. Then, we formulate the problem of representing homogeneous flows with dynamic mode decomposition. In Sec. 3, we describe the adaptation to the sampling rate of the dynamics, and the S-DMD method that forces the eigenvalues to be real. We demonstrate how our method behaves on homogeneous and monotonic flows, and we show its robustness to noise in Sec. 4. We conclude our work and discuss a few future directions in Sec. 5.

2 Preliminaries

Methods in image processing, based on functional analysis, is usually an optimization problem, compound from fidelity, F , and regularization, R , terms, i.e.

$$G(\psi) = F(\psi - f) + R(\psi).$$

And the solution of $\min_{\psi} \{F(\psi - f) + R(\psi)\}$ is the recovered image. A common fidelity term is L_2 norm of the difference between the processed image, ψ , and the given image, f . Kuijper chose the regularization term as a L_p norm of the gradient of ψ [31]

$$J_p(\psi) = \frac{1}{p} \|\nabla \psi\|^p, \quad (1)$$

known as the p -Dirichlet energy. Thus, we can control the level of the smoothness by choosing p . In addition, Kuijper suggested the following scale space as a filter

$$\psi_t = \Delta_p \psi, \quad \psi(0) = f, \quad (\textbf{p-Flow})$$

where the initial condition, f , is the observed image and $\Delta_p(\cdot)$ is the p -Laplacian operator, defined as

$$\Delta_p(\psi) = \nabla \cdot \{|\nabla \psi|^{p-2} \nabla \psi\}. \quad (2)$$

This flow has a finite support in time for any initial condition when $p \in [1, 2)$. Namely, it reaches its steady state in finite time for an arbitrary f . Moreover, there exists function ϕ that holds

$$\Delta_p(\phi) = \lambda \cdot \phi \quad (3)$$

for some real non-positive number (see discussion [9]). These function are called eigenfunctions. If the initial condition is an eigenfunction of Δ_p then the solution of **(p-Flow)** is variable separated and given by

$$\psi(t) = a(t)\phi = [(1 + (2 - p)\lambda \cdot t)^+]^{\frac{1}{2-p}} \cdot \phi. \quad (4)$$

where $(a)^+ = \max\{0, a\}$. This kind of solution we term as *shape preserving flow*. And since λ non-positive and when $p \in [1, 2)$, one can calculate exactly what is the extinction time by (see Fig. 1)

$$T = \frac{1}{\lambda(p-2)}. \quad (5)$$

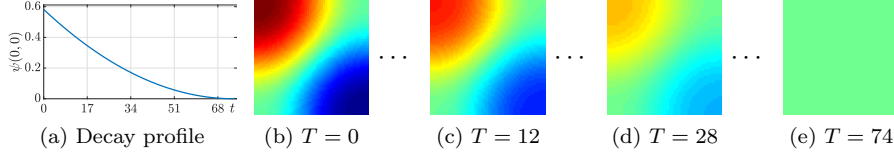


Figure 1: **The solution of $\psi_t = \Delta_p \psi$ initialized with an eigenfunction** ($p = 1.5$, $\lambda = -0.0269$). Left to right: (a) The change over the time of the solution, (4), at the spatial point $(0, 0)$, (b)-(e) snapshots of the solution, ψ , at different points of time.

In general, all the discussion above is valid for any γ -homogeneous operator when $\gamma \in [0, 1)$, when γ -homogeneous operator holds

$$P(a \cdot \psi) = a|a|^{\gamma-1} \cdot P(\psi), \quad (6)$$

for any $a \in \mathbb{R}$. The p -Laplacian operator is private case of γ -homogeneous operator, when $\gamma = p - 1$.

2.1 The p -framework

The p -framework is based on the decay profile of the p -flow, eq. (4). This framework includes transform, inverse-transform, filtering, and spectrum. These analysis tools are based on the fractional derivatives and integrals of the solution of (**p-Flow**). The fractional derivatives and integrals are with respect to t and of the order of $1/(2-p) + 1$. The transform is the fractional derivative of the solution of the PDE, eq. (**p-Flow**). The inverse-transform is defined by fractional integral of the same order of the transform. The filtering is fractional integral of the transform multiplied by $h(t)$. This function attenuates and enhances the transform in different scales. The spectrum is a function of t , resulted from the inner product between the transform and the image (the initial condition of (**p-Flow**)). For more details we refer the reader to [9].

2.2 Explicit scheme of the p -flow

Applying the standard explicit scheme of the p -flow raise two problems. The first is the step size. Until recently there was not CFL condition that allows to use this scheme. The second problem is when $\nabla\psi$ goes to zero. Then, the relation inside the divergence is not defined. These two problems were solved with regularization (adding small enough ε to the denominator). In that case, the CFL is $dt < (\varepsilon^{2-p})/h^2$ where h is the dimension of the signal [32]. However, this solution harm the analytic solution of the p -flow. Such that, even for eigenfunction as an initial condition the solution is not decay polynomially.

On the other hand, Cohen et al. suggested to split the solution of these problems [30]. The limit of the fraction when $\nabla\psi$ goes to zero they solved with different calculation which avoids the dividing by zero. And as to the step size they put forward a generalized CFL condition. We summarize here their conclusions.

The explicit scheme of the dynamics (**p-Flow**) is given by

$$\psi_{k+1} = \psi_k + \Delta_p(\psi_k) \cdot dt_k, \quad \psi_0 = f, \quad (7)$$

where f is the initial condition. Analysing this scheme, they show empirically that this scheme is stable when the step size dt_k is constant (any constant). Moreover, they proved that this scheme converges to zero with the *adaptive step size policy*, given by

$$dt_k = -\frac{\langle \Delta_p \psi_k, \psi_k \rangle}{\|\Delta_p \psi_k\|^2} \cdot \delta, \quad \delta \in (0, 2). \quad (8)$$

In addition, they found an analytic solution to (7) when the initial condition, f , is eigenfunction. Then, for any step size policy the solution of (7) is give by

$$\psi_k = a_k \cdot f, \quad a_k \in \mathbb{R}. \quad (9)$$

The recurrence relating a_{k+1} to a_k is

$$a_{k+1} = a_k (1 + |a_k|^{p-2} \lambda dt_k), \quad a_0 = 1. \quad (10)$$

In particular, this solution under the adaptive step size policy, eq. (8), is given by

$$a_k = (1 - \delta)^k. \quad (11)$$

2.3 Dynamic Mode Decomposition (DMD)

DMD is an analysis tool, revealing the main spatial structures in a fluid flow. By means of these structures, termed as modes, we can describe the entire dynamics. In what following, we summarize the main steps in the standard DMD [7]. Note, that we denote vectors with bullet font and matrices with capital letters.

Forming data matrices The data is a sequence of $N + 1$ snapshots of the dynamic, denoted by $\{\psi_k\}_{k=0}^N$. Each sample from this sequence, ψ_k , belongs to \mathbb{R}^M . Form this sequence, we form two $M \times N$ matrices that the i th column in one matrix is preceding to the i th column to the other, i.e.,

$$\begin{aligned}\Psi_0^{N-1} &= [\psi_0 \quad \dots \quad \psi_{N-1}] \\ \Psi_1^N &= [\psi_1 \quad \dots \quad \psi_N].\end{aligned}\tag{12}$$

Dimensionality reduction It is presumption, the data can be represented concisely but accurately with much lower dimension. Based on this assumption, Schmid used the *Singular Vector Decomposition* (SVD) to represent the matrix Ψ_0^{N-1} ; namely, decomposed this matrix as $\Psi_0^{N-1} = U\Sigma V^*$ where Σ is a diagonal matrix and the dimensions of U, Σ, V are $M \times N$, $N \times N$ and $N \times N$, respectively. The superscript $*$ denotes the conjugate transpose operator.

In this work, we denote as U_r and V_r as the submatrices, containing the first r columns of U and V , respectively; and Σ_r is the a submatrix of Σ , containing the first r rows and columns of Σ . And the dimensionality reduction of the data is defined as

$$X = U_r^* \Psi_0^{N-1}, \quad Y = U_r^* \Psi_1^N.\tag{13}$$

Then, the dimensionality reduced of the $k + 1$ th snapshot is $x_k = U_r^* \psi_k$.

Mode, spectrum and coordination calculation The relation between X and Y can be approximated as,

$$Y \approx F \cdot X,\tag{14}$$

where $F = X_1^N \cdot V_r \cdot \Sigma_r^{-1}$, termed as the *DMD matrix*. Then, the $k + 1$ th sample can be expressed as

$$\mathbf{x}_k \approx F^k \cdot \mathbf{x}_0.\tag{15}$$

If the matrix F is diagonalizable, i.e. can be written as $F = V D W$ where the columns of V , $\{\mathbf{v}_i\}_1^r$, are the right eigenvectors of F , D is a diagonal matrix containing the eigenvalues and the rows of W , $\{\mathbf{w}^i\}_1^r$, are the left eigenvectors of F . And in addition, the relation between V and W is $W = V^{-1}$. Thus, we can expand \mathbf{x}_k back to ψ_k by $\psi_k = U_r \mathbf{x}_k$. These identities and eq. (15) yields

$$\begin{aligned}\psi_k &\approx U_r \cdot \mathbf{x}_k = U_r \cdot V D^k W \mathbf{x}_0 \\ &= U_r \cdot [\mathbf{v}_1 \quad \dots \quad \mathbf{v}_r] \cdot \begin{bmatrix} \mu_1^k & & 0 \\ & \ddots & \\ 0 & & \mu_r^k \end{bmatrix} \cdot \begin{bmatrix} \mathbf{w}^1 \\ \vdots \\ \mathbf{w}^r \end{bmatrix} \cdot \mathbf{x}_0.\end{aligned}\tag{16}$$

The definitions of the modes, spectrum and coordinates result from eq. (16). The modes, denoted by $\{\phi_i\}$, are defined as

$$\Phi = [\phi_1 \quad \dots \quad \phi_r] = U_r \cdot [\mathbf{v}_1 \quad \dots \quad \mathbf{v}_r].$$

The eigenvalues of F , $\{\mu_i\}_{i=1}^r$, is the spectrum of the dynamics. The coordinates are $\boldsymbol{\alpha}^T = [\alpha_1, \dots, \alpha_r]$, where $\alpha_i = \mathbf{w}^i \cdot \mathbf{x}_0$. The following algorithm, Algo. 1, summarizes the procedure of DMD.

Algorithm 1 Standard DMD [7]

- 1: Data sequence $\{\psi_k\}_0^{N+1}$
- 2: Arrange the data into matrices

$$\Psi_0^N \triangleq [\psi_0 \ \cdots \ \psi_N], \quad \Psi_1^{N+1} \triangleq [\psi_1 \ \cdots \ \psi_{N+1}].$$

- 3: Compute the *Singular Vector Decomposition* (SVD) of Ψ_0^N (see [33]), writing

$$\Psi_0^N = U \Sigma V^*.$$

- 4: Dimensionality reduction. Reformulate the data matrices, Ψ_0^N , Ψ_1^{N+1} with the first r singular vectors from the matrix, U

$$X = U_r^* \cdot \Psi_0^N, \quad Y = U_r^* \cdot \Psi_1^{N+1}$$

where U_r contains the first r columns of U and $*$ denotes the conjugate transpose operator.

- 5: Define the matrix F as

$$F \triangleq U_r' \Psi_1^{N+1} V_r \Sigma_r^{-1}.$$

where U_r is $n \times r$, Σ_r is diagonal and $r \times r$, V_r is $r \times r$.

- 6: Compute eigenvalues, μ , and right and left eigenvectors, \mathbf{v} , \mathbf{w} of F , the corresponding modes $\boldsymbol{\phi}$, and the corresponding coordinates α

$$F\mathbf{v} = \mu\mathbf{v}, \quad \mathbf{w}F = \mu\mathbf{w}, \quad \boldsymbol{\phi} \triangleq U_r\mathbf{v}, \quad \alpha \triangleq \mathbf{w}U_r^*\boldsymbol{\psi}_0.$$

- 7: **Outputs:**

$$\{\mu_i, \boldsymbol{\phi}_i, \alpha_i\}_1^r$$

3 DMD for homogeneous and decreasing dynamics

In this section, we formulate a mode decomposition for flows that are governed by a homogeneous operator whose associated spectrum is real-valued. We will first show that DMD can not faithfully represent the dynamics of a γ -homogeneous operator $\gamma \in [0, 1)$, and we discuss an adaptation to the dynamics which allows for such a decomposition. We will then propose a modification to the baseline DMD approach to account for real-valued spectra even when noisy data samples are provided.

3.1 DMD for a homogeneous flow

The dynamic mode decomposition method makes two underlying assumptions. First, the nonlinear dynamics can be represented linearly after dimensionality reduction and second, the data are uniformly sampled in time. Therefore, we can formulate the dynamics as defined in Alg. 1, State 5 [7]. Moreover, we can decompose a given initial condition as a linear combination of the eigenvectors of F . The above structure allows Askham and Kutz [17] to interpret DMD as an exponential fitting problem where the data are linear combinations of eigenvectors scaled by powers of the corresponding eigenvalues.

Other advanced algorithms of DMD lean only on one assumption, the linearity of the latent structure, whilst the data is sampled arbitrarily (known or unknown time points) [19, 18]. The underlying presumption in these articles is that the data is a linear combination of exponential functions. However, to best of our knowledge, no attention was drawn to flow that inherently can not be represented as a summation of exponential functions, for example, dynamics with finite support in time. This is emphasized in dynamics of the (**p-Flow**), where the decay profile is polynomial (Eq. (4)). Moreover, if the PDE (**p-Flow**) is initialised with an eigenfunction, trying to find a linear mapping to this nonlinear dynamics is doomed to failure. Namely, the DMD algorithm is ill pose since the Moore-Penrose pseudoinverse operator will be applied on a matrix with high condition number (analytically it should be infinite). This state holds even if after dimensionality reduction to any order. This problem is demonstrated in the following proposition.

Proposition 1 (DMD an arbitrarily sampled p -flow, initialized with an eigenfunction). *If the p -flow is initialized with an eigenfunction then there is no linear mapping that relates Ψ_0^{N-1} to Ψ_1^N , unless $\{a_k\}$ is a geometric series.*

Proof. Let us examine only three snapshots, $[\psi_0, \psi_1, \psi_2]$. According to the linear mapping $A\psi_0 = \psi_1 = \psi_0 \cdot a_1$. On the other hand, according to (9) the constrain $A\psi_1 = \psi_2 = a_1 A\psi_0 = \psi_0 \cdot a_1^2$ leads to $a_2 = a_1^2$. Therefore, to avoid inconsistent constraints the series $\{a_k\}$ must be geometric. \square

Thus, the dynamic (9) can not be represented as a linear system unless the recurrence relating a_{k+1} to a_k (eq. (10)) is geometric. This recurrence is geometric under the adaptive step size policy (eq. (8)) [30]. And the solution of the explicit scheme is given by $\psi_k = \psi_0 \cdot (1 - \delta)^k$.

Proposition 2 (DMD of the p -flow, sampled adaptively and initialized with eigenfunction). *If the p -flow is initialized with an eigenfunction and the time sampling, dt_k , is (8), then the eigenvalues are on circle with radius $r = 1 - \delta$ and only one mode is not zero.*

Proof. Given relation $A\Psi_0^{N-1} = \Psi_1^N$ we can rewrite it as

$$A\Psi_0^{N-1} = \Psi_1^N = \Psi_0^{N-1} \cdot C = \Psi_0^{N-1} \begin{bmatrix} 0 & 0 & \cdots & 0 & (1 - \delta)^N \\ 1 & 0 & \cdots & 0 & 0 \\ 0 & 1 & \cdots & 0 & 0 \\ \vdots & & \ddots & & \vdots \\ 0 & 0 & \cdots & 1 & 0 \end{bmatrix}. \quad (17)$$

The characteristic polynomial of the matrix C is

$$\begin{aligned} |C - \lambda \cdot I| &= -\lambda \begin{vmatrix} -\lambda & \cdots & 0 & 0 \\ 1 & \cdots & 0 & 0 \\ \vdots & \ddots & \vdots & \vdots \\ 0 & \cdots & 1 & -\lambda \end{vmatrix} + (-1)^{N-1}(1-\delta)^N \begin{vmatrix} 1 & -\lambda & \cdots & 0 \\ 0 & 1 & \ddots & \vdots \\ \vdots & \ddots & \ddots & -\lambda \\ 0 & 0 & \cdots & 1 \end{vmatrix} \\ &= (-\lambda)^N + (-1)^{N-1}(1-\delta)^N \end{aligned}$$

The eigenvalues of C , which are also the eigenvalues of the matrix A , are given by

$$\lambda_i = (1-\delta) \cdot e^{j \frac{2\pi}{N} i}, \quad i = 0, \dots, (N-1).$$

And the corresponding eigenvectors are

$$\tilde{\mathbf{v}}_i = \sqrt{\frac{(1-\delta)^2 - 1}{(1-\delta)^{2N} - 1}} \begin{bmatrix} (1-\delta)^{N-1} \cdot e^{j \frac{2\pi(N-1)}{N} i} & \cdots & (1-\delta) \cdot e^{j \frac{2\pi}{N} i} & 1 \end{bmatrix}^T$$

As discussed in [34] an eigenvector of A is given by $\mathbf{v}_i = \Psi_0^{N-1} \tilde{\mathbf{v}}_i$. Thus, these eigenvector are

$$\begin{aligned} \mathbf{v}_i &= \Psi_0^{N-1} \tilde{\mathbf{v}}_i = \psi_0 \begin{bmatrix} 1, (1-\delta), \dots, (1-\delta)^{N-1} \end{bmatrix} \cdot \\ &\quad \sqrt{\frac{(1-\delta)^2 - 1}{(1-\delta)^{2N} - 1}} \begin{bmatrix} (1-\delta)^{N-1} \cdot e^{j \frac{2\pi(N-1)}{N} i} & \cdots & (1-\delta) \cdot e^{j \frac{2\pi}{N} i} & 1 \end{bmatrix}^T \\ &= \psi_0 \sqrt{\frac{(1-\delta)^2 - 1}{(1-\delta)^{2N} - 1}} (1-\delta)^{N-1} [1 \quad \cdots \quad 1] \cdot \begin{bmatrix} e^{j \frac{2\pi(N-1)}{N} i} & \cdots & e^{j \frac{2\pi}{N} i} & 1 \end{bmatrix}^T \\ &= N \sqrt{\frac{\delta^2 - 1}{\delta^{2N} - 1}} \delta^{N-1} \cdot \begin{cases} \psi_0, & \text{if } i = 0 \\ 0, & \text{otherwise} \end{cases}. \end{aligned}$$

□

Discussion As a result from this proposition, the linearity of the system is not necessary to the DMD to recover the system precisely. The exponential decay profile is enough in this case. Moreover, we can see that a adaptive step size policy is essential to DMD in dynamics derived from γ -homogeneous operator. Although the proof is done on p -Laplacian operator this is correct to any γ -homogeneous operator, not only for $\gamma \in [0, 1)$ but for any value of γ and the proof is trivial.

Generally, in continuous time, not only solutions of linear systems can be expressed as a summation of exponential functions. For example, one-homogeneous operators may induce exponential decay solution. The decay profile depends on the homogeneity order of the operator [10]. If the initial condition, ψ_0 , is an eigenfunction then the decay profile is polynomial when $\gamma \in [0, 1)$, hyperbolic when $\gamma > 1$ and exponential when $\gamma = 1$. However, non linear rescaling of the time variable makes this flow decays exponentially for any value of γ . For instance, we can rescale the time variable for the p -flow by multiplying the p -Laplacian operator by

$$\lambda_\psi^{-1} = -\langle \Delta_p \psi, \psi \rangle / \|\Delta_p \psi\|^2. \quad (18)$$

Then, the new p -flow, termed as the *adaptive p -flow*, is defined by

$$\psi_t = G(\psi), \quad \psi(0) = f, \quad (\text{Adap-Flow})$$

where

$$G(\psi) = \lambda_\psi^{-1} \cdot \Delta_p \psi = -\frac{\langle \Delta_p \psi, \psi \rangle}{\|\Delta_p \psi\|^2} \Delta_p \psi.$$

One can see that the operator $G(\cdot)$ is one-homogeneous. Therefore, if the f is an eigenfunction then the solution of **(Adap-Flow)** decays exponentially. Note, that λ_ψ is generalized Rayleigh quotient, as discussed in [30]. In the following theorem, we list some attributes of the solution of **(Adap-Flow)**.

Theorem 1 (Decay profile and convergence of the adaptive p -flow). *Let $J_p(\psi)$ and $\psi(t)$ be the p -Dirichlet energy and the solution of **(Adap-Flow)**. Then,*

1. J_p converges to zero exponentially.
2. If the initial condition, f , is an eigenfunction of G the solution is $\psi(t) = f \cdot e^{-t}$.
3. For an arbitrary initial condition, f , every element from f decays exponentially.

Proof.

1. Using the chain rule of Brezis [35], we can write

$$\frac{d}{dt} J_p(\psi) = \langle -\Delta_p \psi, \psi_t \rangle = \langle -\Delta_p \psi, -\frac{\langle \Delta_p \psi, \psi \rangle}{\|\Delta_p \psi\|^2} \Delta_p \psi \rangle = -p J_p(\psi).$$

Therefore, $J_p(\psi(t)) = J_p(\psi(0)) \cdot e^{-p \cdot t} = J_p(f) \cdot e^{-p \cdot t}$.

2. The operator $G(\cdot)$ from eq. **(Adap-Flow)** is a one-homogeneous operator. Moreover, if f is an eigenfunction of G then the corresponding eigenvalue equals one. Then, the solution is [9] $\psi(t) = f \cdot e^{-t}$.
3. According to triangle inequality we can say that

$$J_p(f) \cdot e^{-p t} = \frac{1}{p} \|\nabla \psi(t)\|^p = \frac{1}{p} \left\| \nabla \sum_i \phi_i(t) \right\|^p \leq \sum_i \frac{1}{p} \|\nabla \phi_i(t)\|^p = e^{-p t} \cdot \sum_i J_p(\phi_i).$$

Therefore, every element, ϕ_i , decays exponentially.

□

3.2 DMD for a symmetric operator

According to the Theo. 1, third branch, one can conclude that every part of the initial condition, f , decays exponentially under the adaptive step size policy. This decay is monotonically without any oscillations. In addition, it was discussed in [30] that the adaptive step size flow can yield negative eigenvalues but not complex. Thus, the demand on the DMD matrix to be symmetric and real is called for (a symmetric and real matrix has real eigenvalues).

This demand coincides with the analytic expression of non-linear diffusion in [36, chapter 3.4]. In this monograph, Weickert investigated the following nonlinear ODE

$$\psi_t = \nabla \cdot D(\nabla \psi) \nabla \psi$$

where D is a tensor $\mathbb{R}^{2 \times 2} \rightarrow \mathbb{R}^{2 \times 2}$ for continuous and semi-continuous settings. Weickert showed that it is possible to construct a semi-continuous model from this ODE that holds the following

$$\psi_{k+1} = A(\psi_k)\psi_k$$

where $A(\cdot)$ is symmetry.

However, the DMD matrix, F (Algo. 1, state 5), is not limited to be symmetric. If F is symmetric, we can say that this matrix is of the form of (see Appen. A)

$$F = B^T B. \quad (19)$$

By mean of this formulation of F , we can embed this demand in the standard DMD. The following algorithm, Algo. 2, summarizes the DMD for real eigenvalues.

Algorithm 2 *Symmetric DMD* (S-DMD)

1: **Inputs:**

Data sequence $\{\psi_k\}_0^{N+1}$

2: Arrange the data into matrices

$$\Psi_0^N \triangleq [\psi_0 \ \cdots \ \psi_N], \quad \Psi_1^{N+1} \triangleq [\psi_1 \ \cdots \ \psi_{N+1}].$$

3: Compute the *Singular Vector Decomposition* (SVD) of Ψ_0^N (see [33]), writing

$$\Psi_0^N = U \Sigma V^*.$$

4: Dimensionality reduction. Reformulate the data matrices, Ψ_0^N, Ψ_1^{N+1} with the first r singular vectors from the matrix, U

$$X = U_r^* \cdot \Psi_0^N, \quad Y = U_r^* \cdot \Psi_1^{N+1}$$

where U_r contains the first r columns of U .

5: Find the best linear mapping, F , between X and Y in the sense of (see Appen. A)

$$\min_F \|Y - FX\|_F^2, \quad s.t. \quad F = B^T B.$$

6: Compute eigenvalues $\{\mu_i\}_1^r$ and right and left eigenvectors, $\{\mathbf{v}_i\}_1^r \ \{\mathbf{w}^i\}_1^r$, of F , the corresponding modes $\{\phi_i\}_1^r$, and the corresponding coordinates $\{\alpha_i\}_1^r$, writing

$$F\mathbf{v}_i = \mu_i \mathbf{v}_i, \quad \mathbf{w}^i F = \mu_i \mathbf{w}^i, \quad \phi_i \triangleq U_r \mathbf{v}_i, \quad \alpha_i \triangleq \mathbf{w}^i U_r^* \psi_0.$$

7: **Outputs:**

$$\{\mu_i, \phi_i, \alpha_i\}_1^r$$

3.3 p -Decomposition using S-DMD

The explicit scheme of the adaptive p -flow is defined as

$$\psi_{k+1} = \psi_k - \frac{\langle \Delta_p \psi_k, \psi_k \rangle}{\|\Delta_p \psi_k\|^2} \Delta_p \psi_k \cdot \delta, \quad \psi_0 = f, \delta \in (0, 2). \quad (20)$$

Note, that the ψ_k is not bold since this is a general case of snapshot. Using Algo. 2, we can approximate this dynamic by

$$x_k = F^k \cdot x_0, \quad (21)$$

where F is the DMD matrix, x_k and x_0 are the samples ψ_k and ψ_0 in coordination of the columns of U_r , respectively. Thus, we can say that the dynamic can be approximated by

$$\psi_k \approx A^k \cdot \psi_0 \quad (22)$$

where A is defined as $A = U_r \cdot F \cdot U_r^*$ and ψ_0 is the initial condition. Moreover, it is almost easy to see that the modes, ϕ , are the eigenvectors of the matrix A with the same eigenvalues. We can write

$$A\phi = U_r F U_r' U_r v = U_r F v = \mu U_r v = \mu\phi.$$

On the other hand, the matrix A approximates the dynamics, described in (20). Comparing between these expressions, we can rewrite

$$\mu\phi = A\phi \approx \phi - \frac{\langle \Delta_p \phi, \phi \rangle}{\|\Delta_p \phi\|^2} \Delta_p \phi \cdot \delta. \quad (23)$$

We can rephrase this equation as follows

$$\Delta_p \phi \approx \frac{1 - \mu}{\delta} \frac{\|\Delta_p \phi\|^2}{\langle \Delta_p \phi, \phi \rangle} \phi. \quad (24)$$

Then, we can say that ϕ is an approximation of an eigenfunction of the p -Laplacian operator and the corresponding “eigenvalue”, λ , is

$$\lambda = \frac{1 - \mu}{\delta} \frac{\|\Delta_p \phi\|^2}{\langle \Delta_p \phi, \phi \rangle}. \quad (25)$$

Thus, we can relate this mode to an “extinction” time, according to eq. (5).

To recap, we can approximate the p -decomposition, formulated in [9]. Using the S-DMD with rescaled time axis, we can match a mode to an “extinction” time. By mean of that, we can define the discrete spectrum, where the horizon axis of the spectrum is the extinction time of the mode and the vertical axis is the coordinate related to the mode. Here, we reformulate the p -framework, using the aforementioned approximation.

Definition 1 (Discrete p -decomposition). *The discrete p -decomposition of an image f is the set modes $\{\phi_i, T_i, \alpha_i\}_{i=1}^r$.*

As discussed above, the initial condition, f , can be approximated as $\hat{f} = \sum_i \alpha_i \phi_i$. The error, $\|f - \hat{f}\|$, depends on the dimensionality, r [37]. Note, that $\{\phi_i\}_1^r$ is an orthogonal set. Therefore, if the error is zero then this decomposition holds the Parseval’s identity. Namely, we can say $\|f\|^2 = \sum_i |\alpha_i|^2$.

Definition 2 (Discrete p -spectrum). *The discrete p -spectrum of an image f is the set, $\{T_i, |\alpha_i|^2\}_{i=1}^r$, where T_i and α_i are the extinction time and the coefficient of the mode ϕ_i , respectively.*

Definition 3 (Discrete p -filtering). *The discrete p -filtering is amplification (or attenuation) of modes, i.e. the filtered image f_h is given by*

$$f_h = \sum_{i=1}^r \phi_i \alpha_i h_i. \quad (26)$$

4 Results

In this section, we demonstrate the contributions of this article and exhibit the theory we discuss above. First, we examine the robustness to noise of the S-DMD compared to DMD [7], tlsDMD [21] and fbDMD [23]. Then, We showcase the results from Theo. 2 by applying the adaptive step size policy on the p -flow. Then, we implement the discrete p -framework via S-DMD. We compare between the running time of p -decomposition, introduced in [9], and the discrete p -decomposition Def. 2

Symmetric DMD (S-DMD) Here, we implement the S-DMD on a discrete stable linear system

$$\psi_{k+1} = \begin{bmatrix} 0.1 & 0.6 \\ 0.6 & 0.1 \end{bmatrix} \psi_k. \quad (27)$$

The eigenvalues are $\lambda_{1,2} = -0.5, 0.7$ and the initial condition is a normalized summation of the eigenvectors (namely $[1, 0]^T$). We approximate the eigenvalues of this system based on 8 snapshots in presence of white Gaussian noise. We repeat our experiment $N = 1000$ times and average of each of the methods. In Fig. 2 we showcase the results and plot the ellipses which enclose the region of 95% of the estimates that are closest to the true eigenvalue for each of the techniques (see [23]). One can see that for this kind of systems, DMD is superior on the tlsDMD and the fbDMD. In particular, a method that takes into account the system and its inverse is doomed to fail for every stable system since the inverse system is not stable. Therefore, whilst the fbDMD has good performances when the roots are on the unit cycle (BIBO stability) it fails when the roots are in the unit cycle.

DMD derived from the adaptive step size policy Let us recall that the solution of the p -flow decays polynomially when it is initialized with an eigenfunction (see Fig. 1). And Theorem 1 shows that with a scale time policy the decay is exponential. Moreover, according to Prop. 2 is enough only one nonzero mode to describe accurately the solution of p -flow initialised with an eigenfunction.

We show these conclusions in Fig. 3. The Y -axes is the p -spectrum and the X -axes is the time index. One can see that the power of the mode is almost exactly the power of the initial condition, f . This power is given in the “extinction” time of this mode, which coincides with the analytic solution (eq. (5)).

Discrete p -Framework Here, we demonstrate the discrete decomposition we formulate in Def. 1. This decomposition, containing the triplets mode-time-coefficient $\{\phi_i, T_i, \alpha_i\}_i^r$, approximates the entire solution of (p-Flow). The approximation is a summation of a finite set of exponential functions. Each function is characterized with

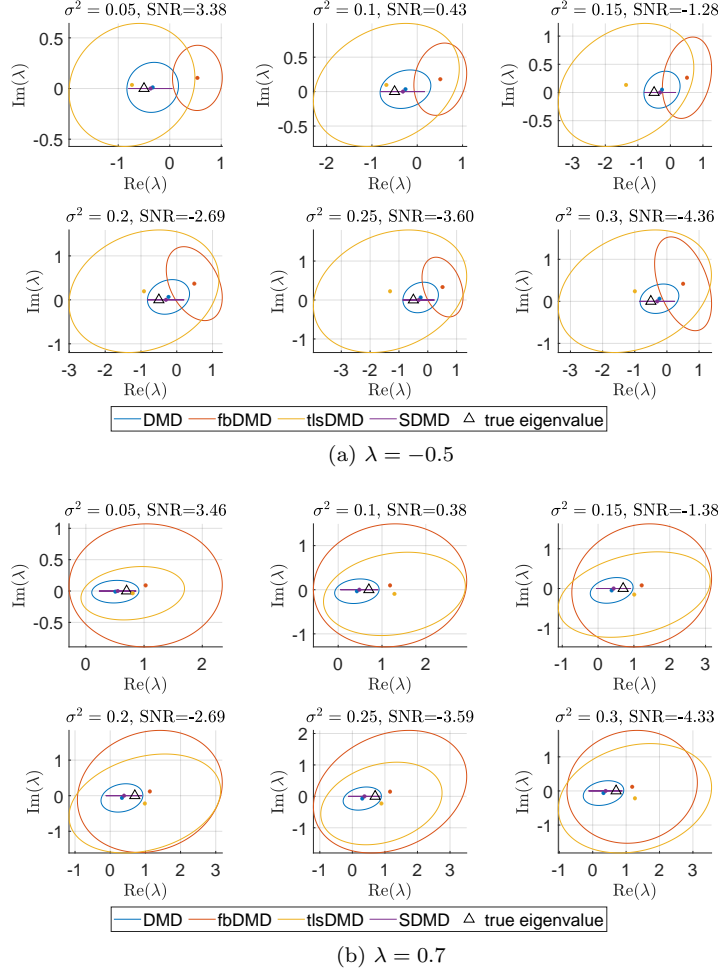


Figure 2: We compare DMD [7], tlsDMD [21], fbDMD [23] and S-DMD based on their approximation for the eigenvalue of system (27) when various levels of noise are introduced, $-4 \leq SNR \leq 4$.

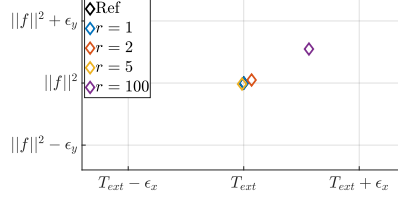


Figure 3: *Discrete p-Spectra* - The X -axes is the time variable and the Y -axes indicate the power of the eigenfunction's spectrum. The power is finite and equal to the power of the eigenfunction, f . The axis are between $T_{ext} \pm \epsilon_x$ and $\|f\|^2 \pm \epsilon_y$ where $\epsilon_x = 2 \cdot 10^{-6}$ and $\epsilon_y = 4 \cdot 10^{-5}$.

a shape (mode), decay rate (“extinction time”), and power (coefficient). Following these definitions we formulate the spectrum in Def. 2.

We demonstrate this decomposition on the image in Fig. 7a with $p = 1.01$. We bring here the p -decomposition to this image for $p = 1.01$ (Fig. 4), firstly shown in [9]. We bring it here as a reference to the approximated decomposition. The p -spectrum,

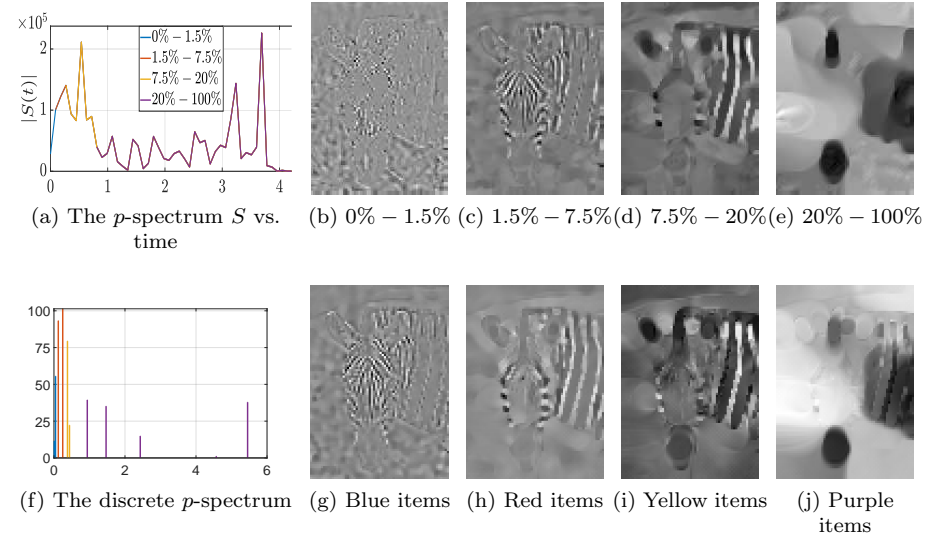


Figure 4: First row, zebra image decomposition with $p = 1.01$. Second row, approximated decomposition of the zebra image for $p = 1.01$ via S-DMD

defined in Def. 2, is shown in Fig. 4a. Then, the Figs. 4b-4e are disjoint parts of the image. Each image represents different part of the spectrum. The image in Fig. 4b represents the all parts in the spectrum in the segment $t \in [0, 0.063]$ (the blue part). The image in Fig. 4c represents the all parts in the spectrum in the segment $t \in [0.063, 0.315]$ (the red part). Similarly, the images in Figs. 4d and 4e are related to the segments $t \in [0.315, 0.84]$ and $t \in [0.84, 4.2]$ (the yellow and the purple parts).

The approximation of this decomposition with the same value of p is shown in Fig.

4. The discrete spectrum is shown in Fig. 4f. The X and Y axes indicate the time index and the power (squared coefficient) of the modes. Namely, the spectrum is the set of points $\{T_i, \alpha_i^2\}_i^r$. Then, we split the spectrum to four groups. The first part contains all the modes, whose “extinction time” hold $T_i \in [0, 0.063]$ (the blue part in the spectrum). This part of the spectrum is shown Fig. 4g. The second group, shown in Fig. 4h, contains all the modes with “extinction time” in the segment $[0.063, 0.315]$ (the red part in the spectrum). In the same way, the images in Figs. 4i and 4j contain the mode with “extinction time” in $[0.315, 0.84]$ and $[0.84, 6]$ (yellow and purple parts in the spectrum), respectively. Generally, one can see that the S-DMD algorithm “fits” the texture and small scale components in the image to small “extinction time”.

Run time Vs. Image size The most prominent advantage of this method is the running time. The p -decomposition requires evaluating the (**p-Flow**) with uniform step size, which limit to small step size (the step size depends on the accuracy level). Then, for every pixel in the image fractional derivative is calculated. This might involve FFT and IFFT for every point in the image. In Fig. 5, we show the change rate in the computation time versus the size of the image. The X -axis indicates the

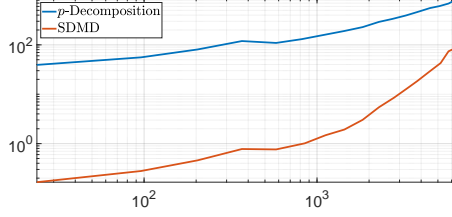


Figure 5: Running time Vs. Image size

size of the image (number of pixels) in log scale and Y -axis indicates the running time for compute the p -spectrum in log scale. It seems that the running time increasing exponentially with the image size. However, the running time of the approximated p -decomposition is smaller than the accurate one in at least order of magnitude.

Discrete p -filtering The last part of the discrete p -decomposition we would like to demonstrate here is the discrete filtering, formulated in Def. 3. In Fig. 6 we

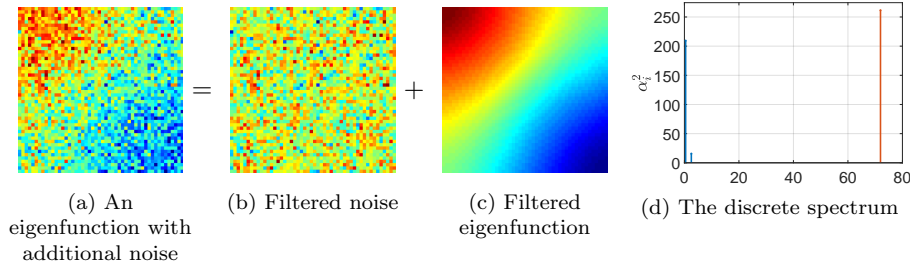


Figure 6: filtering

demonstrate filtering with S-DMD. The initial condition (Fig. 6a) is an eigenfunction, $\lambda = -0.0269$, $p = 1.5$, with additional noise, $N \sim \mathcal{N}(0, 0.3)$. The discrete spectrum is brought in Fig. 6d. One can see that different scales of the signal are represented in different places in the time axes. In Figs. 6b and 6c, we show the the blue and the red parts of the spectrum.

We test this algorithm again on a natural image (Fig. 7a). We corrupt the image with additional noise, $N \sim \mathcal{N}(0, 0.2)$, $SNR = 3.8175dB$ (Fig. 7b) . Filtering out the modes with the lower “extinction time”, we get the result in Fig. 7c. As expected, we

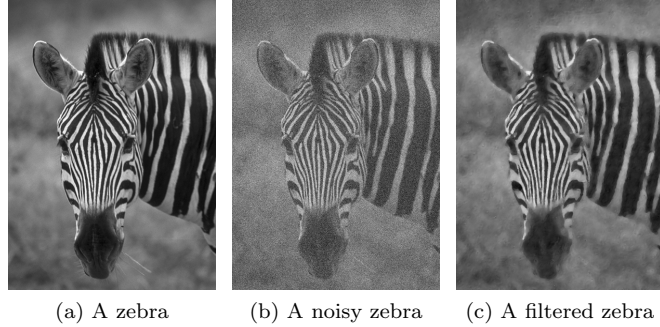


Figure 7: *Denoiser* - Using the definition of filtering, Def. 3, we filter out the noise.

lose some small details but the texture in general is preserved.

5 Conclusion

In this work, we introduce time rescaling to γ -homogeneous flow. This enables to implement the DMD on these flows. This rescale is essential to DMD and causes this decomposition to be much more accurate and even to recover the entire flow identically. In addition, we formulate the *Symmetric DMD* (S-DMD) to force the DMD matrix to be symmetric.

These two adaptations, the time rescale and the S-DMD, allow us to formulate the p -framework approximation. This framework leans on the solution of (**p-Flow**), which is $p - 1$ -homogeneous and symmetric. The adaptations of the sampling rate and to the DMD spectrum answer the these two attributes of the p -flow. Thus, we can approximate the p -decomposition, avoiding the numeric fractional derivative, necessary to this decomposition.

List of Symbols

| | |
|--------------------------|---|
| P | Dynamical System |
| ψ_k | The system state in the k th step in \mathbb{C}^M |
| Ψ_0^{N-1}, Ψ_1^N | $[\psi_0, \dots, \psi_{N-1}], [\psi_1, \dots, \psi_N]$ |
| A | $M \times M$ matrix, approximating a linear mapping between Ψ_0^{N-1} and Ψ_1^N |
| U, Σ, V | <i>Singular Vector Decomposition</i> (SVD) of Ψ_0^{N-1} |
| X, Y | dimensional reduced of Ψ_0^{N-1}, Ψ_1^N , respectively |

| | |
|--|--|
| F_r | $r \times r$ matrix, approximating a linear mapping between X and Y |
| \mathbf{v}_i | column vector, the i th right eigenvectors of F |
| \mathbf{w}^i | row column, the i th left eigenvectors of F |
| $D = \text{diag}\{\mu_1, \dots, \mu_r\}$ | $\{\mu_i\}_1^r$ are eigenvalues of F . |
| $\Phi = [\phi_1, \dots, \phi_r]$ | $\{\phi_i\}_1^r$ are the modes of the dynamics. |
| $\alpha^T = [\alpha_1, \dots, \alpha_r]$ | $\{\alpha_i\}_1^r$ are the coordinates of the modes $\{\phi_i\}_1^r$ respectively. |
| J_p | The p -Dirichlet energy |
| Δ_p | The p Laplacian operator |
| \mathcal{P} | The p -transform |
| \mathcal{P}^{-1} | The inverse p -transform |
| \mathcal{S} | The p -Spectrum |

A Finding a symmetric DMD matrix

We are looking for linear mapping, F , between X and Y when the mapping is symmetric, i.e.

$$\min_F \|Y - FX\|_F^2, \quad s.t. \quad F = F^T. \quad (28)$$

In addition, according to spectral theorem every symmetric real matrix can be diagonalized. Therefore, we can express the matrix as $F = Q^T D Q$ when Q and D are orthogonal and diagonal matrices. Then, we can take squared root of the matrix D and rewrite this expression as $F = Q^T \sqrt{D^T} \sqrt{D} Q$. Then, we can reformulate the optimization problem as

$$\min_F \|Y - FX\|_F^2, \quad s.t. \quad F = B^T B. \quad (29)$$

Note, that B is over the complex field and T denotes for the transform operator. Embedding the constrain in the optimization expression, we get

$$\min_B \|Y - B^T B X\|_F^2.$$

Using $\|Y - B^T B X\|_F^2 = \text{Tr}\{Y - B^T B X\}^T \{Y - B^T B X\}$ and the derivatives

$$\begin{aligned} \frac{\partial}{\partial B} \text{Tr}\{FBG\} &= F^T G^T \\ \frac{\partial}{\partial B} \text{Tr}\{FB^T G\} &= GF, \end{aligned}$$

we get that the minimizer, B , holds

$$B^T B X X^T + X X^T B^T B = X Y^T + Y X^T.$$

Substituting $B^T B$ with F , we get that the minimizer, F , of (28) holds the following Sylvester equation

$$F X X^T + X X^T F = X Y^T + Y X^T. \quad (30)$$

References

- [1] Shai Biton, Nadav Arbel, Gilad Drozdov, Guy Gilboa, and Amir Rosenthal. Optoacoustic model-based inversion using anisotropic adaptive total-variation regularization. *Photoacoustics*, 16:100142, 2019.
- [2] Yuya Ohmichi. Preconditioned dynamic mode decomposition and mode selection algorithms for large datasets using incremental proper orthogonal decomposition. *AIP Advances*, 7(7):075318, 2017.
- [3] Damian Kaliroff and Guy Gilboa. Self-supervised unconstrained illumination invariant representation. *arXiv preprint arXiv:1911.12641*, 2019.
- [4] Uri Shaham, Kelly Stanton, Henry Li, Boaz Nadler, Ronen Basri, and Yuval Kluger. Spectralnet: Spectral clustering using deep neural networks. *arXiv preprint arXiv:1801.01587*, 2018.
- [5] Tamar Rott Shaham, Tali Dekel, and Tomer Michaeli. Singan: Learning a generative model from a single natural image. In *Proceedings of the IEEE International Conference on Computer Vision*, pages 4570–4580, 2019.

- [6] Martin Burger, Guy Gilboa, Michael Moeller, Lina Eckardt, and Daniel Cremers. Spectral decompositions using one-homogeneous functionals. *SIAM Journal on Imaging Sciences*, 9(3):1374–1408, 2016.
- [7] Peter J Schmid. Dynamic mode decomposition of numerical and experimental data. *Journal of fluid mechanics*, 656:5–28, 2010.
- [8] Da Kuang, P Jeffrey Brantingham, and Andrea L Bertozzi. Crime topic modeling. *Crime Science*, 6(1):12, 2017.
- [9] Ido Cohen and Guy Gilboa. Introducing the p-laplacian spectra. *Signal Processing*, 167, 2020.
- [10] Ido Cohen and Guy Gilboa. Shape Preserving Flows and the p–Laplacian Spectra. working paper or preprint, October 2018.
- [11] Guy Gilboa. A spectral approach to total variation. In *International Conference on Scale Space and Variational Methods in Computer Vision*, pages 36–47. Springer, 2013.
- [12] Guy Gilboa. A total variation spectral framework for scale and texture analysis. *SIAM journal on Imaging Sciences*, 7(4):1937–1961, 2014.
- [13] Oren Katzir. On the scale-space of filters and their applications. Master’s thesis, Technion — Israel Institute of Technology, Haifa 3200003, March 2017.
- [14] Guy Gilboa. *Nonlinear Eigenproblems in Image Processing and Computer Vision*. Springer, 2018.
- [15] Bernard O Koopman. Hamiltonian systems and transformation in hilbert space. *Proceedings of the national academy of sciences of the united states of america*, 17(5):315, 1931.
- [16] Igor Mezić. Spectral properties of dynamical systems, model reduction and decompositions. *Nonlinear Dynamics*, 41(1-3):309–325, 2005.
- [17] Travis Askham and J Nathan Kutz. Variable projection methods for an optimized dynamic mode decomposition. *SIAM Journal on Applied Dynamical Systems*, 17(1):380–416, 2018.
- [18] Romain Leroux and Laurent Cordier. Dynamic mode decomposition for non-uniformly sampled data. *Experiments in Fluids*, 57(5):94, 2016.
- [19] Florimond Guéniat, Lionel Mathelin, and Luc R Pastur. A dynamic mode decomposition approach for large and arbitrarily sampled systems. *Physics of Fluids*, 27(2):025113, 2015.
- [20] J Nathan Kutz, Steven L Brunton, Bingni W Brunton, and Joshua L Proctor. *Dynamic mode decomposition: data-driven modeling of complex systems*. SIAM, 2016.
- [21] Maziar S Hemati, Clarence W Rowley, Eric A Deem, and Louis N Cattafesta. De-biasing the dynamic mode decomposition for applied koopman spectral analysis of noisy datasets. *Theoretical and Computational Fluid Dynamics*, 31(4):349–368, 2017.
- [22] Shervin Bagheri. Effects of small noise on the dmd/koopman spectrum. *Bulletin Am. Phys. Soc.*, 58(18):H35, 2013.
- [23] Scott TM Dawson, Maziar S Hemati, Matthew O Williams, and Clarence W Rowley. Characterizing and correcting for the effect of sensor noise in the dynamic mode decomposition. *Experiments in Fluids*, 57(3):42, 2016.

- [24] Omri Azencot, Wotao Yin, and Andrea Bertozzi. Consistent dynamic mode decomposition. *SIAM Journal on Applied Dynamical Systems*, 18(3):1565–1585, 2019.
- [25] Taku Nonomura, Hisaichi Shibata, and Ryoji Takaki. Dynamic mode decomposition using a kalman filter for parameter estimation. *AIP Advances*, 8(10):105106, 2018.
- [26] Taku Nonomura, Hisaichi Shibata, and Ryoji Takaki. Extended-kalman-filter-based dynamic mode decomposition for simultaneous system identification and denoising. *PloS one*, 14(2), 2019.
- [27] Matthew O Williams, Ioannis G Kevrekidis, and Clarence W Rowley. A data-driven approximation of the koopman operator: Extending dynamic mode decomposition. *Journal of Nonlinear Science*, 25(6):1307–1346, 2015.
- [28] Qianxiao Li, Felix Dietrich, Erik M Boltt, and Ioannis G Kevrekidis. Extended dynamic mode decomposition with dictionary learning: A data-driven adaptive spectral decomposition of the koopman operator. *Chaos: An Interdisciplinary Journal of Nonlinear Science*, 27(10):103111, 2017.
- [29] Omri Azencot, N Benjamin Erichson, Vanessa Lin, and Michael W Mahoney. Forecasting sequential data using consistent koopman autoencoders. *arXiv preprint arXiv:2003.02236*, 2020.
- [30] Ido Cohen, Adi Falik, and Guy Gilboa. Stable explicit p-laplacian flows based on nonlinear eigenvalue analysis. In *International Conference on Scale Space and Variational Methods in Computer Vision*, pages 315–327. Springer, 2019.
- [31] Arjan Kuijper. p-laplacian driven image processing. In *2007 IEEE International Conference on Image Processing*, volume 5, pages V–257. IEEE, 2007.
- [32] George Baravdish, Olof Svensson, and Freddie Åström. On backward p (x)-parabolic equations for image enhancement. *Numerical Functional Analysis and Optimization*, 36(2):147–168, 2015.
- [33] Lloyd N Trefethen and David Bau III. *Numerical linear algebra*, volume 50. Siam, 1997.
- [34] Clarence W Rowley, Igor Mezić, Shervin Bagheri, Philipp Schlatter, and Dan S Henningson. Spectral analysis of nonlinear flows. *Journal of fluid mechanics*, 641:115–127, 2009.
- [35] Haim Brezis. *Opérateurs maximaux monotones et semi-groupes de contractions dans les espaces de Hilbert*, volume 5. Elsevier, 1973.
- [36] Joachim Weickert. *Anisotropic diffusion in image processing*, volume 1. Teubner Stuttgart, 1998.
- [37] Matan Gavish and David L Donoho. The optimal hard threshold for singular values is $4/\sqrt{3}$. *IEEE Transactions on Information Theory*, 60(8):5040–5053, 2014.